

JPMTR-2216
DOI 10.14622/JPMTR-2216
UDC 004.93|77.05|7.02

Research paper | 171
Received: 2022-06-29
Accepted: 2022-12-27

Use of ArUco markers for image registration of photographs and influence of camera tilt on process performance

Veronika Štampfl and Jure Ahtik

Chair of Information and Graphic Arts Technology,
Department of Textiles, Graphic Arts and Design,
Faculty of Natural Sciences and Engineering, Ljubljana, Slovenia

veronika.stampfl@ntf.uni-lj.si
jure.ahtik@ntf.uni-lj.si

Abstract

Image registration is widely used in the field of graphic technology, from printing processes to research. In order to successfully align two images, image sections must be recognized. In printing, simple linear markers can be used for alignment, while advanced visual systems use fiducial markers, such as ArUco markers, for specific position recognition. These can be applied to any surface and are quickly recognized by open-source algorithms. This gives us the ability to recognize any visually perceived surface and align it with the target image. This research focuses on the applicability of ArUco markers as reference points for image registration of photographs of flat, uniform surfaces. The camera tilt position was adjusted in four combinations to mimic the imperfect positioning of the camera relative to the observed surface. Twelve marker combinations were tested, varying in size, number, and positioning. Research has shown that ArUco markers are suitable as reference points for image registration, but in specific combination of size and position. General guidelines for their use have been established.

Keywords: position registration, photo-alignment, pattern recognition, fiducial markers

1. Introduction

Image registration is an important part of various processes in graphic technology. Most commonly, it is used to align separations during the printing process, where the operator interacts with the press to achieve perfect alignment of the separations and thus sharp colour reproduction (Kipphan, 2001). During print quality control, certain visual systems can monitor the quality of prints or even the press itself. Image registration is later on used to combine data from different cameras or overlap the acquired data with intended result (Villalba-Diez, et al., 2019). In postpress, for example in packaging, the technician checks the alignment of printed sheet according to the positioning marker and sets the CNC cutting device accordingly (Esko-Graphics Kongsberg AS, 2018).

Another important example of the use of image alignment in graphic technology is any type of research where data acquisition is done with imaging systems such as cameras and microscopes (Štampfl and Ahtik, 2022; Leskovšek, et al., 2019). Consumer-based cameras are often used in research purposes since photography is an approachable technique for capturing visual data.

While performing image analysis of captured data, a comparison of two images is often needed to extract different data between two stages within the research. If maintaining camera position in relation to observed scene is not possible, image registration is mandatory, since it enables image alignment and further comparison of sequential images. Captured images can be manually aligned based on our visual perception, but in cases with a large number of images, automatic alignment methods are applicable. Image registration in these cases is based on certain image features or predefined areas, such as fiducial markers (Zakiev, et al., 2020).

With camera equipment evolving, integrated software takes care of the most critical settings to get an appropriately exposed image. This often eliminates the necessary understanding of ISO, white balance, aperture, and shutter speed settings, and even having the ability to focus on the desired point. However, influences of spherical and chromatic aberrations, colour profiles of the device, properties of lighting, its position, and the position of the camera are often overlooked or are not given enough attention (Ray, 2002; Opaka, et al., 2013; Kim, et al., 2011; Jackman, 2010; Keskinen, et al., 2019).

In this research, we determine the performance of ArUco markers as orientation points for image registration of photographs of flat surfaces, and the influence of camera inclination on the performance of open-source image registration algorithm when using ArUco markers as reference points. Different combinations of markers' positions, their amount and size are tested under different camera inclinations and guidelines are proposed.

2. Image registration and markers

Alignment of images is present in all research areas that deal with image processing in some way. When registering images, we always need a reference image to serve as a target for aligning the test image. Through registration, we can compose images into larger images, which we call mosaicing, we can overlay images taken at different times and thus monitor changes, we can overlay them with reference models and ensure that the product matches the desired values, or we can overlay images taken with different devices, i.e., sensors (Cosman, 2012).

The images are written as a function of two values, $f(x, y)$, where the x and y coordinates are in 2D space and f is the intensity or pixel intensity. The pixel intensity of a greyscale image is also called the greyscale value, while colour images consist of as many images as there are channels. Thus, the RGB colour image consists of three images, each representing one of the colour channels R, G, and B, and represented as a greyscale image. Numerically, images are written as matrices of the values of the individual pixels. By calculating the transformation matrix of the test image, it is aligned with the reference image (Gonzales, Woods and Eddins, 2004).

There are several types of image deformation (Figure 1). Translation moves an area so that a straight line is mapped into a straight line with the same orientation and distance between the same pairs of points. Rotation rotates the area, changing the direction of the lines while keeping the distance the same. Scaling changes the distance between two points on the sur-

face while the direction remains the same. The affine transformation includes all three of the above deformations as well as the directional deformation of the shape. The lines remain parallel, but the shape is no longer the same. One such example is a rectangle that transforms into a parallelogram. To align such a deformation, we need at least three markers in each image. In the bilinear transformation, the straight lines are preserved, but the image is mapped conically. We need four points on each image to align them. This type of mapping is also called homography (Hladnik and Muck, 2010; Kamoun and Joslove, 2019).

Methods for registering images in the image domain are, in general, divided into sparse and dense methods (Zhang, et al., 2019), also found under feature-based methods and area-based methods (Zitová and Flusser, 2003). In sparse methods, the main points, i.e., the features, are extracted from the reference and test images and the transformation matrix is determined based on the detected coordinates. Lines, such as edges, are most commonly used to align images, as are point features, such as corners, line cross sections, and the centroids of larger surfaces. Deshmukh and Bhosle (2011) therefore name these methods as point-mapping methods. The most common are corners, which can be selected manually or detected automatically via various algorithms, such as features from accelerated segment test (FAST), scale-invariant feature transform (SIFT), speeded-up robust features (SURF), and ORB, which is a combination of oriented FAST and rotated binary robust independent elementary features (BRIEF) (Zhang, et al., 2019).

Dense methods, unlike sparse, do not first search for points common to the reference and test images, but check the degree of similarity of each pixel of the reference and test images using methods to describe similarities or differences across the image. Therefore, they are also named area-based methods. After calculating the similarity of the image pairs, a transformation matrix is created, and the similarity indices are recalculated. Various similarity evaluation methods have been proposed, such as mutual information (MI), normalized cross-correlation coefficient (NCC), root-

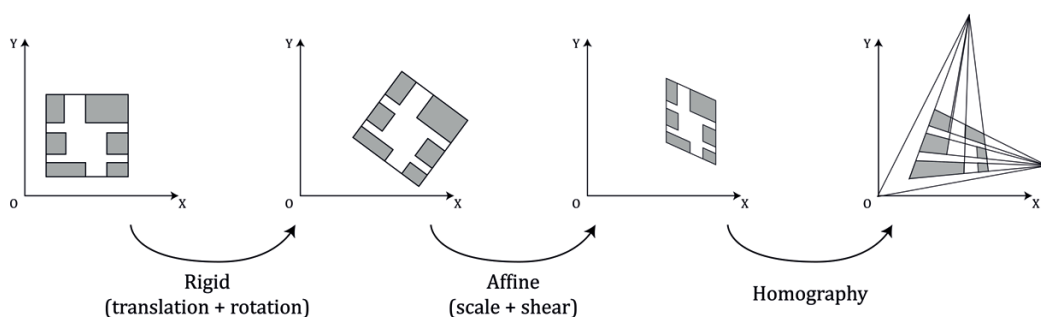


Figure 1: Types of image deformations (Kamoun and Joslove, 2019)



Figure 2: Fiducial marker types: Intersense (a), CyberCode (b), VisualCode (c), ReactIVision (d), ARToolKit (e), Matrix (f), ARTag (g), ARToolKit Plus (h), AprilTags (i), ArUco (j) (Garrido-Jurado, et al., 2016)

mean-square-error (RMSE), and peak signal to noise ratio (PSNR). However, it should be noted that the latter two methods are highly dependent on the uniformity of illumination and may provide unusable results for unevenly illuminated test surfaces. The final transformation matrix is difficult to determine precisely, so artificial intelligence methods are used for this purpose (Zitová and Flusser, 2003; Zhang, et al., 2019).

In some cases, histogram equalisation can be used to increase image contrast and allow better detection of key elements for image registration and further analysis. In their study, Kumar Mondal, Chatterjee and Tudu (2021) demonstrate the quality of histogram equalisation methods and algorithms using Fourier spectrum analysis of greyscale test images and their binarization.

Fiducial markers were originally developed for augmented reality, where systems are used to identify and track visual areas. The use of markers has expanded to other areas, particularly robotics and drones, where markers must be robust and detectable by visual systems, economically accessible, and capable of accurate detection in 3D space (Lightbody, Krajník and Hanheide, 2017). They consist of unique patterns that, in combination with the associated algorithm, enable the identification of individual marks. The algorithms are adapted to each type of label as they differ in size, resolution, and shape (Fiala, 2010). The most common is the use of square markers with a black border, which improves the quality and speed of their recognition. Their greatest advantage is the four corner points, which allow their position to be determined quickly and easily, and often a single marker is sufficient for identification. Some types of the most common markers are shown in Figure 2 (Garrido-Jurado, et al., 2016).

3. Methods

This experiment was designed to evaluate whether ArUco markers are an appropriate tool to set up as registration markers on the surfaces of our research lab, which is often used as testing environment for capturing visual data where image registration is needed for further image analysis. Twelve combinations of markers' size, position and quantity were tested along with four camera inclinations, in order to determine the influence of inaccurate sensor position on the performance of image registration with ArUco markers.

3.1 Markers and reference images

ArUco markers allow their fast generation and detection via already established algorithms, which a user can control with code written in Python programming language. It is also possible to determine the dimensions of the markers and the size of the matrix containing them (OpenCV, 2022). In the experiment we used markers from the already existing *aruco.DICT_6x6_250* dictionary, which is available in open-source library OpenCV. We used the first six markers, labelled with IDs 0, 1, 2, 3, 4, and 5, with an internal marker matrix of 6×6 bits and 700 pixels per side, generated using Python.

Generated ArUco markers in various combinations of size, number, and position, as shown in Table 1, were arranged on A4 faces, the centre points of markers being 3 cm away from the edge of the paper sheet, 24 cm apart in x direction and 16 cm apart in y direction. The layouts were exported as PNG images, which were used as reference images for image registration in this experiment. A set of reference images can be seen in Figure 3.



Figure 3: Reference images for image registration; first row large markers: 2L_DIAG (a), 2L_LEFT (b), 2L_TOP (c), 4L (d), 5L (e), and 6L (f); in second row small markers (marked S instead of L as in Table 1)

Table 1: Marker combinations

Label	Size [mm]	Number of markers	Position
2L_DIAG	22	2	diagonally
2L_LEFT	22	2	left corners
2L_TOP	22	2	upper corners
4L	22	4	all corners
5L	22	5	all corners and centre
6L	22	6	all corners and additional marker on top and bottom
2S_DIAG	15	2	diagonally
2S_LEFT	15	2	left corners
2S_TOP	15	2	upper corners
4S	15	4	all corners
5S	15	5	all corners and centre
6S	15	6	all corners and additional marker on top and bottom

3.2 Test surfaces and image capture

To determine the success of aligning the test photographs with the reference images, we added a grid of dark squares to the latter. The comparison can be seen in Figures 4a and 4b. The files were exported to PDF formats, which were printed on A4 office paper using a Canon imageRUNNER 2530i printer. This produced a series of test surfaces, which were placed on a platform that allowed for tilt adjustment. We tested four inclination combinations of the platform by 10° along the x -axis (long edge) and y -axis (short edge). The combinations are listed in Table 2.

To calculate the differences between the aligned images and the reference surfaces, we reduced the saturation of the print files (Figure 4c) and saved them as PNG files. This was necessary because the printed files did not reach the same level of saturation as it was set in the print file.

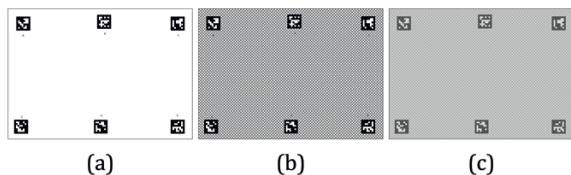


Figure 4: Reference image for image alignment (a), printing pattern (b), and reference image for calculating the degree of registration (c)

To illuminate the test areas, we used an LED strip with a colour temperature of 2700 K. Its shape corresponded to the shape of the test surface, and it was positioned 10 cm above the surface, which provided

uniform illumination of the surface from above. Four series of photographs of 12 marker combinations were photographed with a Nikon D850 camera and a Nikkor 50 mm 1:1.4G lens at the same settings and a distance of 82 cm from the centre of the surface.

Table 2: Platform inclination combinations

Label extension	Inclination on x axis	Inclination on y axis
_REG	0°	0°
_X	10°	0°
_Y	0°	10°
_XY	10°	10°

3.3 Image processing and analysis

We wanted to perform the entire image processing process in one program, which we achieved using the Python programming language and the open-source libraries OpenCV, a collection of various functions and commands in the field of visual perception, the NumPy library, which allows array conversion, RawPy, which as part of the LibRaw libraries allows working with raw photo formats, and Pillow, an abbreviation for Python Imaging Library, which allows editing images.

We generated code that requires RAW photos of test areas, reference images for alignment, and reference images for calculating differences between input data. When we run the program code, it automatically saves intermediate results: generated ArUco markers, images with highlighted detected markers, aligned images, aligned images with equalised histogram, and final difference images. The entire code is divided into separate parts so that individual steps can be executed separately from the others. The individual parts are presented below with key components of the open-source Python code.

The first section of the code consists of import commands for used libraries. It also defines a matrix of strings, which are image names within one folder on a local disk. This enables the code use even with additional test images. In our case, those were strings found in Table 1 under Label.

The second section imports a dictionary of ArUco markers. They are defined, along with their size and quantity, and saved into a local folder. Key code components:

```
aruco.Dictionary_get()
aruco.drawMarker()
```

The third section ensures image registration. Reference image is imported and ArUco markers recognised. Test photographs are converted from RAW format to JPG,

taking into account the white balance setting. On each imported test image, ArUco markers are detected, marked, and saved as separate images, enabling intermediate control of the process. Detected ArUco markers on test images provide reference points, which are aligned to the reference points on the reference image. Transformation matrix is calculated based on reference points alignment and used to align test image to reference image. The aligned image is saved as a new JPG file. Key code components:

```
rawpy.imread()
aruco.detectMarkers()
aruco.drawDetectedMarkers()
cv2.findHomography()
cv2.warpPerspective()
```

The fourth section equalizes histograms of aligned images from the previous section and reference images for difference calculations (Figure 4c). This ensures comparability of images, since the brightest and the darkest part of the image is always found in ArUco marker, which serves as top and bottom threshold. Contrast limited adaptive histogram equalization (CLAHE) algorithm is used. Equalised images are saved for further processing as separate files. Key code components:

```
cv2.createCLAHE()
clahe.apply()
```

Fifth, and the last section of the code, subtracts the aligned images from their reference images, generating image differences. The function compares each pixel of the aligned image with its position on the reference image and returns the absolute difference. Difference images are saved as separate files and the quantities of pixels for each grey value are saved into a CSV file. Key code component:

```
ImageChops.difference
```

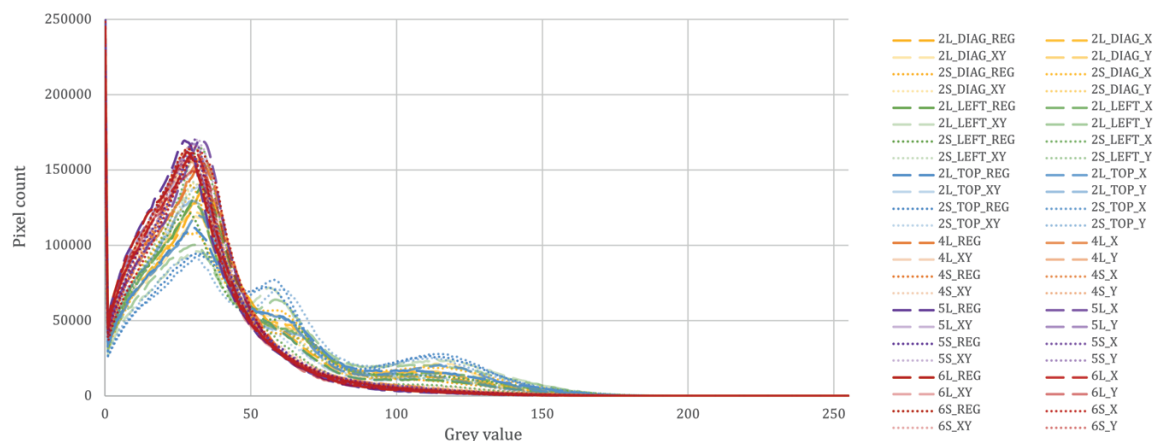


Figure 5: Histograms of difference images

Pixel count for each grey value was plotted for every difference image, along with average pixel count values for each grey level, averaged for ArUco markers combinations and platform inclinations.

4. Results and discussion

The success rate of the tested photo-alignment method was observed by the number of pixels of each value. Black pixels (grey value is 0) indicate a 100 % match between the reference image and the photographed image, while white pixels with a value of 255 indicate a 0 % match. Grey values in between represent partial matches depending on the value.

In Table 3 black pixel counts of the averaged histograms are presented along with the calculated coverage percentage over entire image.

Table 3: Average values of black pixel count and percentage of black pixels

Averaged over	Black pixels Count	Percentage [%]
REG	222 960	3.41
X	185 945	2.85
Y	196 220	3.00
XY	178 677	2.73
S	194 472	2.98
L	197 370	3.02
6	219 122	3.35
5	221 433	3.39
4	211 779	3.24
2_TOP	168 920	2.59
2_LEFT	171 607	2.63
2_DIAG	182 900	2.80

Figure 5 shows the histograms of the difference images for all test photographs. Similar trends can be observed in the histogram shapes, but there are differences in

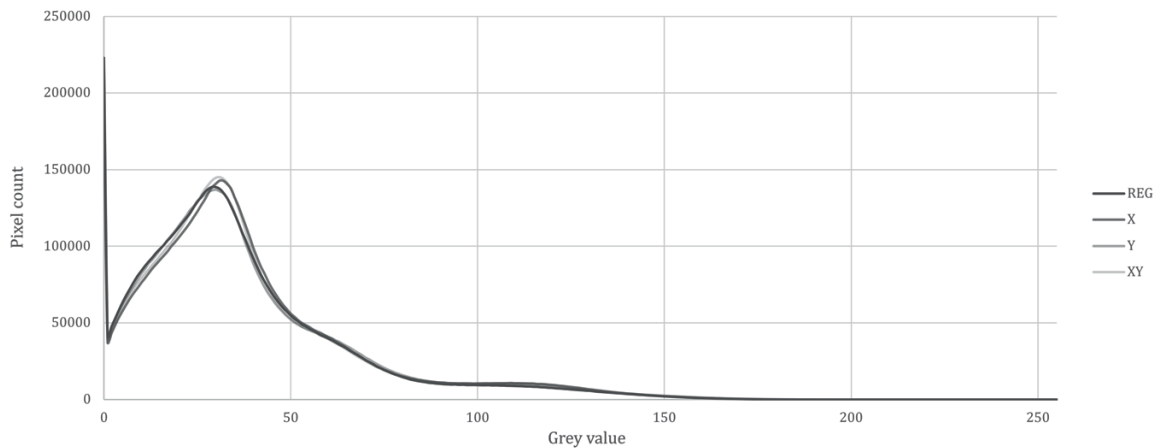


Figure 6: Histograms of averaged values at each grey value for platform inclination combinations

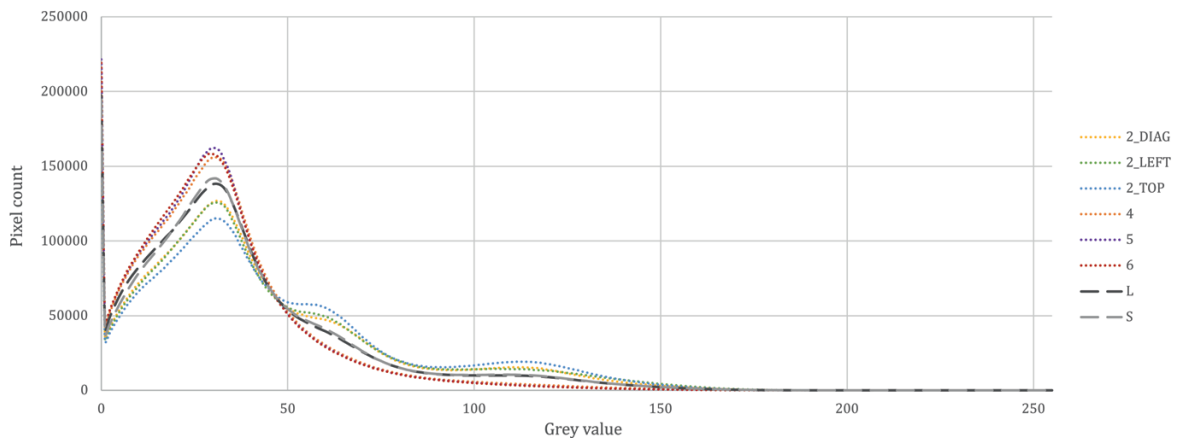


Figure 7: Histograms of averaged values at each grey value for individual marker combinations

the ranges of the function maxima. To better interpret the results, we calculated the average values of the histograms with respect to the observation angle of the photographed area (Figure 6) and individual marker patterns (Figure 7). Further, the number of dark and light pixels was calculated for the images, using the grey value of 50 as the threshold. Coefficient values are numerically presented in Table 4.

Table 4: Slope coefficient of the line between normalised values of pixel sum from grey level 0 to 50 and 51 to 255

	REG	X	Y	XY
S	-0.614	-0.568	-0.574	-0.636
L	-0.655	-0.572	-0.591	-0.569
6	-0.823	-0.798	-0.803	-0.649
5	-0.814	-0.789	-0.793	-0.797
4	-0.683	-0.762	-0.784	-0.726
2_TOP	-0.246	-0.250	-0.292	-0.560
2_LEFT	-0.476	-0.555	-0.348	-0.306
2_DIAG	-0.517	-0.349	-0.476	-0.443

The sums of pixel values for light (grey values 51–255) and dark pixels (grey value 0–50) was normalized and averaged for platform inclination and marker combination. The results are shown in Figure 8a, while in Figure 8b the slope coefficients of the line between normalized values for light and dark pixels are shown.

Figure 6 shows that there is not much difference between four combinations of platform inclinations, i.e., the parallelism of the camera to the photographed surface. This shows that the image registration method used is suitable for image registration of images taken with a camera tilted up to 10° in any plane. The larger number of black pixels (grey value 0) in the difference images corresponds to the lower second peaks of the histograms. Although the trends of all four histograms are similar, we can evaluate the results based only on the number of black pixels. The histograms averaged as REG have 3.41 % black pixels relative to the whole image, while X has 2.85 %, Y has 3.00 %, and XY has 2.73 %. This shows that images without tilt achieve better image registration levels, as the percentage is highest for REG. Instances with tilt across the y-axis (Y) have

0.15 % more black pixels than across the x -axis (X), indicating that image registration is more effective in instances averaged across Y . This is partly due to the different distances of the ArUco markers from the rotation axis. If you compare the coefficients for X and Y from Figure 8b, you can see that more accurate image registration is performed when the markers are further apart in the perpendicular direction to the tilt axis. This is most obvious in the cases with two markers, where 2_TOP and 2_DIAG give better results under condition Y , as one marker is 3 cm away from the tilt axis and the second 27 cm. Under condition X , the markers are 3 cm and 19 cm away from the tilt axis, giving less favourable results. This observation is also confirmed in the measurements for 2_LEFT, where for instance X , where the markers are 3 cm and 19 cm from the tilt axis, the image registration is better than in case Y , where both markers are 3 cm from the tilt axis and their relative distance is zero.

Figure 7 shows the averaged histograms of the difference images with respect to the size, amount, and position of the ArUco markers. Here, S and L represent the average histograms of the small and large markers, respectively. The shape of the histograms shows no obvious differences in the success of image registration as a function of marker size, and the same is true for the number of black pixels. However, a comparison of the coefficients from Figure 8b shows that large markers behave better in cases without tilt, as the coefficient is 0.041 lower than for the combination REG- S , while small markers behave better with tilt in both axes, with XY - S having a coefficient of -0.636 and XY - L -0.569 , a difference of 0.067. With tilt in only one

axis, x or y , there is not much difference between the results, in X only 0.004 in favour of the large markers and 0.017 in Y , again in favour of the same markers.

The averaged histograms from Figure 7 show large differences between the marker combinations with four, five, and six markers and those with only two. Differences can also be seen in the number of black pixels, with 4, 5 and 6 being closer together and forming one group, while 2_TOP, 2_LEFT and 2_DIAG form the second group, with the difference between 4 as the last in its group and 2_DIAG as the first in the other group being 0.44 %. The same trend of differences can be seen in the second peak of the averaged histograms, where the plots for 4, 5 and 6 are almost identical and the remaining three with two markers are much lower. Histograms for 4, 5 and 6 are decreasing gradually after grey level 50, while histograms for 2_TOP, 2_LEFT and 2_DIAG fluctuate. This suggests that image registration is less successful when two markers are used. The reasons for this have already been described in one of the previous sections and show how the position of the markers is also important.

As can be seen from the histograms in Figure 7 and the low coefficient values in Figure 8b, combinations with four, five, and six markers provide the best results regardless of platform tilt, but combinations with five markers provide the most consistent results even with platform tilt in both axes.

Combinations with six markers give the best results when the platform is not tilted or only tilted over one axis, while combinations with four markers show less

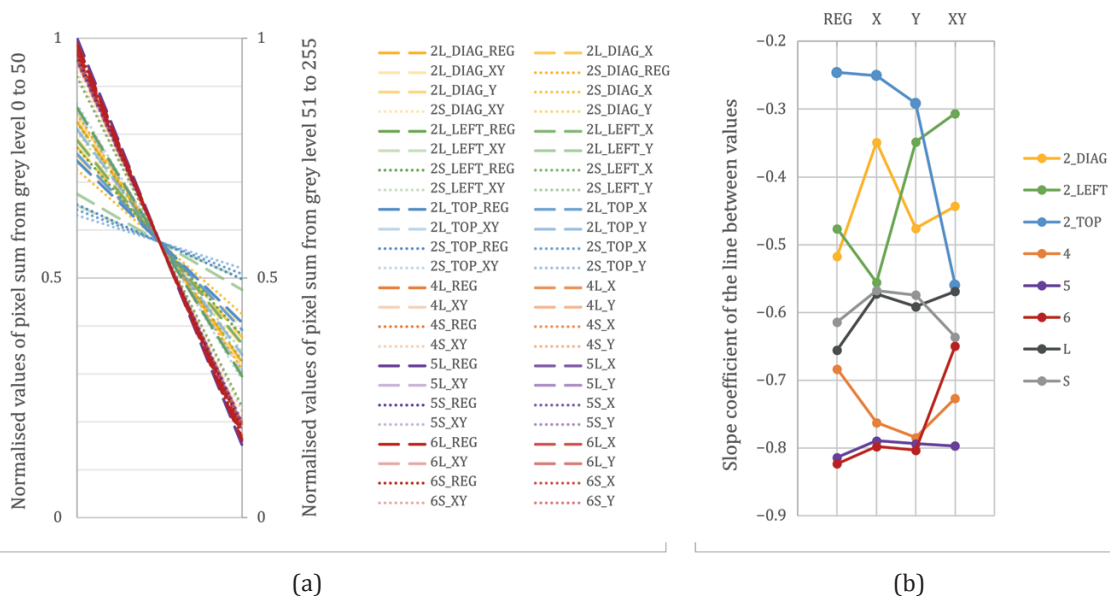


Figure 8: Correlation of normalised values of pixel sums for grey levels 0 to 50 and 51 to 255, respectively (a), and slope coefficient of the line between values (b)

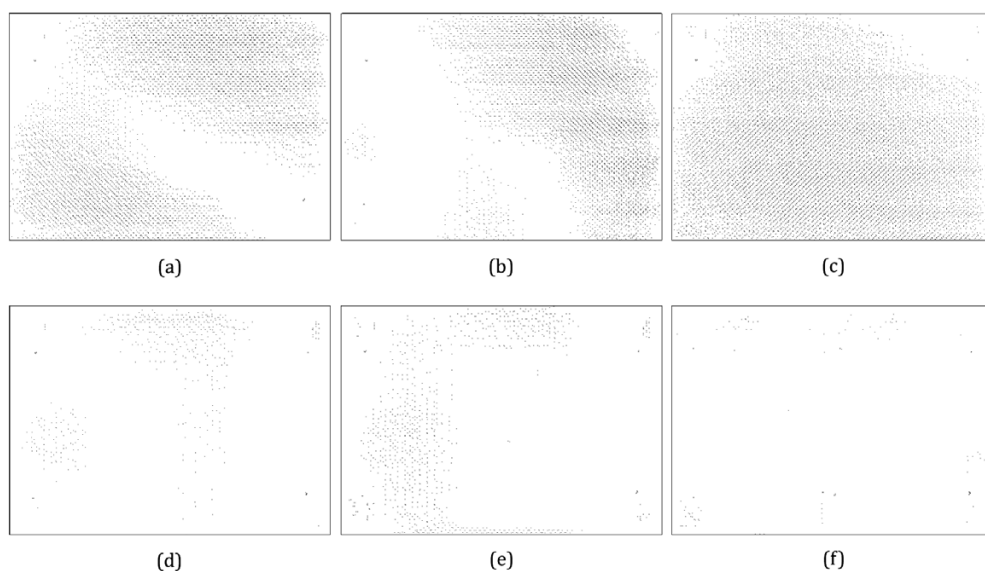


Figure 9: Inverted binarized difference images between reference images and test photos for series REG with large markers: 2L_DIAG (a), 2L_LEFT (b), 2L_TOP (c), 4L (d), 5L (e), and 6L (f)

successful image registration even in cases without platform tilt. This may be related to the fact that we did not use camera calibration methods. Therefore, spherical aberrations may still be present even though we used a lens with settings that ensure minimal aberrations of this type. An additional marker in the centre for marker combinations 5 and two additional markers on the long edges for marker combinations 6 provide intermediate control points that minimise the effect of spherical aberration.

These quantitative results can also be confirmed visually. Figure 9 shows difference images for test photos taken without the platform tilt (REG), using only large ArUco markers (L) for registration. The presented images were binarized at a threshold of 128 and inverted, to illustrate the areas of best image alignment. The black passages show the areas where image registration was less successful, which is especially visible in cases with two markers (Figures 9a, 9b, and 9c). In the 2_DIAG case, a brighter diagonal passage can be seen between the markers, indicating successful registration in that area, while the opposite corners of the image show a lower level of accurate registration. At 2_LEFT, registration is more successful on the left side of the image where the markers are located, while at 2_TOP it is more successful in the upper part of the image, again in the area of the markers, with the registration success rate decreasing with distance from the markers. Four markers provide much more uniform registration of the images, while five markers provide uniform alignment even in the centre of the image. Six markers increase the density of marker surface coverage and produce the most visually aligned image.

5. Conclusion

The study provided quantitative results on the success of the method of using ArUco tags to match photographs with prepared reference images. We found that two ArUco markers were insufficient for high-quality image alignment, regardless of their position on the test surface. Four, five and six markers on the test surface provide more consistent alignment, and the degree of success of the method depends on the position of the markers.

When using four markers, there are some deviations, which is due to the fact that the method is not able to eliminate spherical distortions caused by the photographic system. For this purpose, we suggest either calibrating the camera and including calibration profiles in the method or using a larger number of control points, i.e., markers. The five-marker method shows good results at all angles of image capture, while the most uniform image registration is provided by six ArUco markers, but not when tilted about both axes. Depending on the quantitative results and their confirmation by visual observation of the final images of the differences, we recommend the use of six markers on the observed surface, placed at regular intervals. We also recommend the use of larger markers, as they proved to be more reliable in most of the tested cases.

This method has proven to be efficient in image registration of two samples equipped with a specific array of ArUco markers. It allows the user to easily equip the observed surface with the markers, which can be quickly recognized by an open-source code available to any user.

Acknowledgements

This work was supported by the Slovenian Research Agency (Infrastructural Centre RIC UL-NTF).

References

- Cosman, P., 2012. *Image registration*. [pdf] San Diego, University of California. Available at: <<http://code.ucsd.edu/pcosman/regs2012.pdf>> [Accessed 8 April 2022].
- Deshmukh, M.P. and Bhosle, U., 2011. A survey of image registration. *International Journal of Image Processing*, 5(3), pp. 245–269.
- Esco-Graphics Kongsberg AS, 2018. *User manual for Kongsberg XPA systems*. [pdf] Available at: <https://docs.esko.com/docs/en-us/Kongsberg_XPA/1.1/referenceguide/3168_User_Manual_XPA_us.pdf> [Accessed 24 November 2022].
- Fiala, M., 2010. Designing highly reliable fiducial markers. *IEEE Transactions on Pattern Analysis and Machine Intelligence*, 32(7), pp. 1317–1324. <https://doi.org/10.1109/TPAMI.2009.146>.
- Garrido-Jurado, S., Muñoz-Salinas, R., Madrid-Cuevas, F.J. and Medina-Carnicer, R., 2016. Generation of fiducial marker dictionaries using mixed integer linear programming. *Pattern Recognition*, (51), pp. 481–491. <https://doi.org/10.1016/j.patcog.2015.09.023>.
- Gonzales, R.C., Woods, R.E. and Eddins, S.L., 2004. *Digital image processing using MATLAB*. New Jersey: Pearson Education.
- Hladnik, A. and Muck, T., 2010. *Obdelava digitalnih slik v grafiki, prvi del: osnove*. Ljubljana: Naravoslovnotehniška fakulteta, Oddelek za tekstilstvo.
- Jackman, J., 2010. *Lighting for digital video and television*. 3rd ed. Oxford: Focal press, pp. 96–101.
- Kamoun, E., and Joslove, J., 2019. Image registration: from SIFT to deep learning. *Sicara, Computer vision*, [blog] 16 July. Available at: <<https://www.sicara.ai/blog/2019-07-16-image-registration-deep-learning>> [Accessed 8 April 2022].
- Keskinen, T., Mäkelä, V., Kallioniemi, P., Hakulinen, J., Karhu, J., Ronkainen, K., Mäkelä, J. and Turunen, M., 2019. The effect of camera height, actor behavior, and viewer position on the user experience of 360° videos. In: *IEEE Conference on Virtual Reality and 3D User Interfaces (VR)*. Osaka, Japan, 23–27 March 2019. IEEE, pp. 423–430. <https://doi.org/10.1109/VR.2019.8797843>.
- Kim, U.S., Lee, J.M., Kim, Y.M., Park, K.T. and Moon, Y.S., 2011. Photographic color reproduction based on color variation characteristics of digital camera. *KSII Transactions on Internet and Information Systems*, 5(11), pp. 2160–2174. <https://doi.org/10.3837/tiis.2011.11.016>.
- Kipphan, H. ed., 2001. *Handbook of print media: technologies and production methods*. New York: Springer.
- Kumar Mondal, S., Chatterjee, A. and Tudu, B., 2021. Image contrast enhancement using histogram equalization: a bacteria colony optimization approach. *Journal of Print and Media Technology Research*, 10(2), pp. 95–118. <https://doi.org/10.14622/JPMTR-2103>.
- Leskovšek, M., Stankovič Elesini, U., Škerjanc, A., Vrabc, M., and Gabrijelčič Tomc, H., 2019. Making a 3D model of merino wool fibre with photogrammetric processing of SEM images. In: *MCM2019: proceedings from the 14th Multinational Congress on Microscopy*. Belgrade, Serbia, 15–20 September 2019. Belgrade, Serbia: University of Belgrade, Institute for Biological Research “Siniša Stanković”, National Institute of Republic of Serbia, Serbian Society for Microscopy, pp. 53–55.
- Lightbody, P., Krajník, T. and Hanheide, M., 2017. A versatile high-performance visual fiducial marker detection system with scalable identity encoding. In: *SAC '17: Proceedings of the Symposium on Applied Computing*. Marrakech, Morocco, 3–7 April 2017. New York, NY, USA: Association for Computing Machinery, pp. 376–282. <https://doi.org/10.1145/3019612.3019709>.
- Opaka, U., Javoršek, A., Starešinič, M. and Javoršek, D., 2013. Analysis of colour profile quality for digital camera Nikon D50. *Tekstilec*, 56(2), pp. 123–128. <https://doi.org/10.14502/Tekstilec2013.56.123-128>.
- OpenCV, 2022. *ArUco marker detection*. [online] OpenCV: Open Source Computer Vision. Available at: <https://docs.opencv.org/4.x/d9/d6a/group_aruco.html> [Accessed 24 November 2022].
- Ray, S.F., 2002. *Applied photographic optics: lenses and optical systems for photography, film, video, electronic and digital imaging*. 3rd ed. Routledge.
- Štampfl, V. and Ahtik, J., 2022. The influence of the surrounding space on the lighting conditions in a photographic scene. In: *Proceedings of the 11th International Symposium on Graphic Engineering and Design GRID*. Novi Sad, Serbia, 3–5 November 2022. Novi Sad: University of Novi Sad. pp. 863–871. <https://doi.org/10.24867/GRID-2022-p95>.
- Villalba-Diez, J., Schmidt, D., Gevers, R., Ordieres-Meré, J., Buchwitz, M., and Wellbrock, W., 2019. Deep learning for industrial computer vision quality control in the printing industry 4.0. *Sensors*, 19(18): 3987. <https://doi.org/10.3390/s19183987>.

- Zakiev, A., Tsoy, T., Shabalina, K., Magid, E. and Saha, S.K., 2020. Virtual experiments on ArUco and AprilTag systems comparison for fiducial marker rotation resistance under noisy sensory data. In: *2020 International Joint Conference on Neural Networks*. Glasgow, UK, 19–24 July 2020. IEEE. <https://doi.org/10.1109/IJCNN48605.2020.9207701>.
- Zitová, B. and Flusser, J., 2003. Image registration methods: a survey. *Image and Vision Computing*, 21(11), pp. 977–1000. [https://doi.org/10.1016/S0262-8856\(03\)00137-9](https://doi.org/10.1016/S0262-8856(03)00137-9).
- Zhang, Z., Han, D., Dezert, J. and Yang, Y., 2019. A new image registration algorithm based on evidential reasoning. *Sensors*, 19(5): 1091. <https://doi.org/10.3390/s19051091>.